Open Research Online

The Open University's repository of research publications
and other research outputs

GIADA performance during Rosetta mission scientific operations at comet 67P

Journal Item

For guidance on citations see FAQs.

oro.open.ac.uk

GIADA performance during Rosetta mission scientific operations at comet 67P

R. Sordini[1,*] , V. Della Corte[2,1], A. Rotundi[2,1], S. Rotunno[2], M. Ferrari[1], S.L. Ivanovski[1], L. Colangeli[3], P. Palumbo[2,1], J.J. Lopez-Moreno[4], J. Rodriguez[4], M. Fulle[5], S.F. Green[6], E. Mazzotta-Epifani[7], R. Morales[4], M. Accolla[8], E. Palomba[1], M. Cosi[9], M. Herranz[4], V. Liuzzi[2].

[1]INAF- Istituto di Astrofisica e Planetologia Spaziali, via del Fosso del Cavaliere, 100, Roma 00133, Italy.

[2]Dipartimento di Scienze e Tecnologie, Università degli Studi di Napoli "Parthenope", CDN IC4, Napoli 80143, Italy.

[3]ESA, European Space Research and Technology Centre (ESTEC), Keplerlaan 1, 2201 AZ Noordwijk, The Netherlands.

[4]Instituto de Astrofisica de Andalucia, Consejo Superior de Investigaciones Cientìficas (CSIC), P.O. Box 3008, 18080 Granada, Spain.

[5]INAF-Osservatorio Astronomico di Trieste, Via Tiepolo 11, Trieste, 34143 Italy.

[6]Planetary and Space Sciences, School of Physical Sciences, The Open University, Milton Keynes MK7 6AA, UK.

[7]INAF Osservatorio Astronomico di Roma, Via di Frascati, 33, Monte Porzio Catone, Rome, Italy.

[8]INAF-Osservatorio Astrofisico di Catania, Via S. Sofia 78, Catania 95123 Italy.

[9]Leonardo S.p.A. – Airborne and Space Systems, Via A. Einstein, 35, 50013 - Campi Bisenzio, Firenze, Italy.

Abstract

The Grain Impact Analyser and Dust Accumulator (GIADA) instrument onboard Rosetta studied the dust environment of comet 67P/Churyumov–Gerasimenko from 3.7 au inbound, through perihelion, to 3.8 au outbound, measuring the dust flow and the dynamic properties of individual particles. GIADA is composed of three subsystems: 1) Grain Detection System (GDS); 2) Impact Sensor (IS); and 3) Micro-Balances System (MBS). Monitoring the subsystems' performance during operations is an important element for the correct calibration of scientific measurements. In this paper, we analyse the GIADA inflight calibration data obtained by internal calibration devices for the three subsystems during the period from 1 August 2014 to 31 October 2015. The calibration data testify a nominal behaviour of the instrument during these fifteen months of mission; the only exception is a minor loss of sensitivity for one of the two GDS receivers, attributed to dust contamination.

Keywords: Rosetta ESA Mission; GIADA; Dust instrument; Inflight calibration; Performance monitoring.

1. Introduction

Starting from the 1960s, various types of in-situ dust detectors have been developed and flown on several space missions (McDonnell, 1978) in order to characterise cometary, planetary and interplanetary dust environments. Exploiting various detection techniques, dust instruments were able to measure particle sizes and flux and to provide information on their physical and dynamical properties. Impact ionisation detectors (Auer and Sitte, 1968), mounted onboard Pioneer 8 and 9 (Berger and Richardson, 1969), Heos 2, Helios (Dietzel et al., 1973), Ulysses (Grün et al., 1992a) and Galileo probes (Grün et al., 1992b), provided mass and velocity of the impacting particles, by measuring the charge released from their hypervelocity impact onto a solid target.

---

* Corresponding author:
Roberto Sordini
Email addresses: roberto.sordini@iaps.inaf.it
Phone: +39 0649934117

Penetration detectors, i.e. cells pressurised with gas and equipped with a pressure-monitoring device, were installed on Pioneer 10 and Pioneer 11 probes (Humes, 1980). A particle penetrating the cell generates a gas leakage, with consequent pressure loss recognised as an impact (O'Neal, 1974); this allows measurement of the dust flux. Polyvinylidene fluoride (PVDF) impact sensors were mounted onboard Vega 1 and 2 (Simpson et al., 1987), ARGOS (Tuzzolino et al., 2001) and New Horizons (Horányi et al., 2008) space probes to detect high-velocity particles. Dust particles penetrating the thin PVDF film cause a localised volume depolarisation of the material and consequently a **charge** pulse in an external circuit. The amplitude of the pulse is proportional to the mass and velocity of the penetrating particle (Simpson and Tuzzolino, 1985). Lead zirconate titanate piezoelectric sensors (PZTs) were used on GIOTTO (McDonnell, 1987) and PROBA-1 missions (Leese et. al., 1996). The PZTs are microphones that detect the bending waves produced by a particle impacting onto a target surface and thus measuring the released momentum (McDonnell, 1969). Quartz Crystal Microbalances (QCMs) are used to measure integrated mass flux. The QCMs determine the cumulative mass of sub-micron and micron-sized particles collected on a sensor quartz crystal by measuring the resonance frequency variation with respect to a reference quartz crystal (McKeown, 1998; Sauerbrey, 1959). These sensors were used as dust collectors on Mars Pathfinder Mission (Landis et al., 1996) and as molecular contamination monitoring systems on MSX (Wood et al., 2000) and SDS-4 (Nakamura et al., 2013) satellites, on the Space Shuttle (Soares et al., 2002), and on the International Space Station (Tighe et al., 2009).

Some in-situ dust detectors were developed combining different detection techniques. Notable examples are: the Giotto Dust Impact Detection System, DIDSY (McDonnell, 1987), the CDA onboard Cassini (Srama et al., 2004), the DFMI onboard Stardust (Tuzzolino et al., 2003) and the Grain Impact Analyser and Dust Accumulator (GIADA) (Colangeli et al., 2007) onboard Rosetta (Fig. 1). GIADA combines three different detection subsystems: the Grain Detection System (GDS), able to detect individual dust particles by means of a laser curtain without affecting particle dynamics (Mazzotta Epifani et al., 2002); the Impact Sensor (IS), consisting of five PZT sensors connected to an aluminium plate and measuring the momentum released by an impacting particle (Esposito et al., 2002); the Micro-Balances System (MBS), composed of five QCMs, which measure the cumulative mass of particles smaller than 5 μm in diameter (Palomba et al., 2002).

Launched on 2 March 2004, Rosetta reached the comet 67P/Churyumov–Gerasimenko (67P hereafter) on 6 August 2014; since then it continuously monitored the 67P nucleus and its activity along its orbit from 3.7 au inbound to perihelion (13 August 2015) and outbound to 3.8 au. GIADA detected the first dust particle on 1 August 2014 and since then it monitored the evolution of the 67P dust environment (Della Corte et al., 2015, 2016b; Fulle et al., 2015, 2016a, 2016b; Grün et al., 2016; Rotundi et al., 2015). During the mission, we monitored the functional parameters of the sensors, evaluating their health status and checking their performance over time and in different environmental conditions. The laser emission **intensity** (Pankove, 1968; Xiang et al., 2009) and the QCM **crystals resonance** frequency (Palomba et al., 2002; Soares et al., 2002; Tighe et al., 2009) are sensitive to the operative environmental conditions, e.g. the temperature. The PZT sensors are sensitive to temperature variations (Sabat et al., 2007; Sherrit et al., 1999) and sensor ageing (Berlincourt et al., 2000). Temperature variations are induced by Rosetta spacecraft - Sun distance changes and by specific observational geometries. It is pivotal to monitor the behaviour of the three GIADA subsystems, as done by Della Corte et al. (2014) during the Rosetta cruise phase.

In the present work, we study GIADA performances from the Rosetta rendezvous with comet 67P until a couple of months after perihelion, i.e. from 1 August 2014 to 31 October 2015. The spacecraft thermal conditions, mainly influenced by the heliocentric distance, represent one of the most critical aspect that can affect GIADA performances. In order to monitor the subsystems behaviour in the entire range of temperatures faced by GIADA, we selected the inflight calibration data acquired every hour during the inbound branch orbit, i.e. with Rosetta escorting comet 67P while approaching perihelion. As a confirmation of the thermal behaviour results, we also included a small portion of the outbound orbit, i.e. about
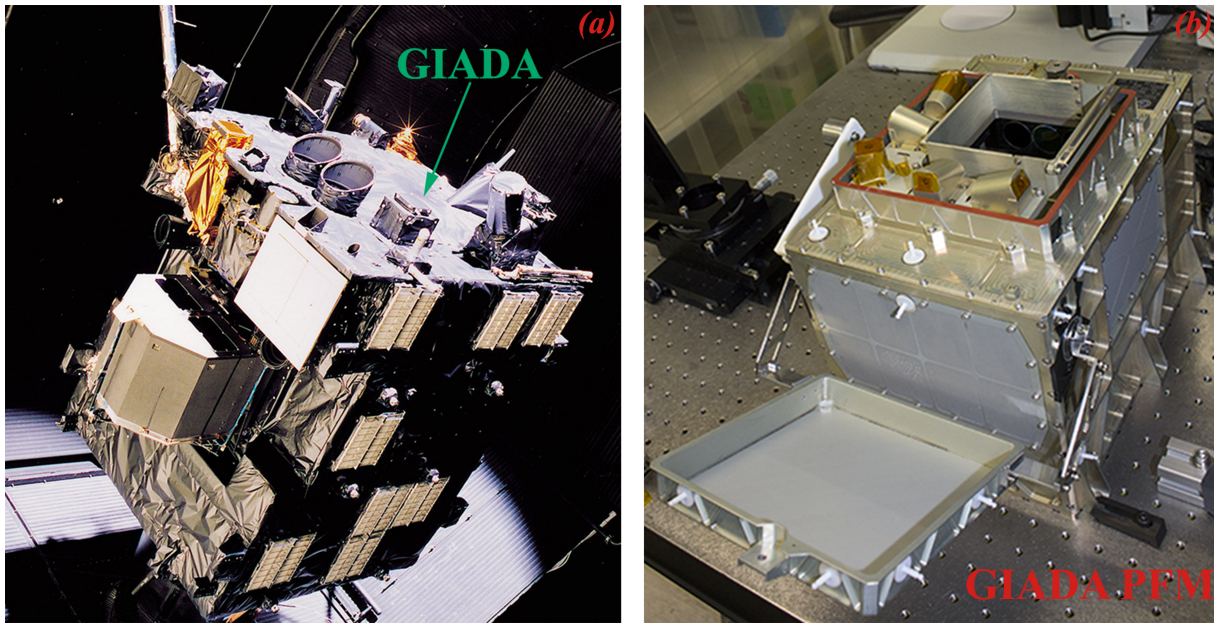
two months and a half after perihelion.

Fig. 1: *(a)* GIADA, installed on the nadir panel of the Rosetta spacecraft, during the thermal test performed in 2002 in the Large Space Simulator at ESA's ESTEC facility, The Netherlands (Photo: ESA/A. Van Der Geest). *(b)* GIADA Proto Flight Model (GIADA PFM), operating in a clean room in our laboratory.

2. GIADA subsystems

The GIADA instrument and its performances are described in Colangeli et al. (2007) and in Della Corte et al. (2014), here we recall the main characteristics of the sensors of the three GIADA subsystems. The GDS is made up of four SDLO-4001 InGaAs CW (continuous-wave) laser diodes (λ= 915 nm), operated **in pair pulsed mode at 100 kHz, i.e. four lasers are switched on/off two by two at 100 kHz (Mazzotta Epifani et al., 2002),** creating a 100 mm x 100 mm x 3 mm laser curtain (Fig. 2). Each laser module is equipped with a thermistor and a photodiode, to monitor the laser diode temperature and the output light signal, reported in the subsystem's housekeeping telemetries. A system of mirrors (periscope group) deflects the laser beam outside GIADA through a slit. The two GDS receivers (Left and Right receivers) are made of two series of four PIN photodiodes, mod AME AE-945, coupled with Winston cones (used as collimating optics), and placed at 90° with respect to the laser source. In front of each cone an interference filter is installed to optimise the transmission of the radiation peaked at λ=915 nm (Mazzotta Epifani et al., 2002). The GDS receivers and the proximity electronics have been designed and built to minimise the effects induced by temperature changes and stray light. Stray light is minimised by double subtraction, that removes the spurious common-mode light, and capacitive coupling that cuts the continuous contribution (Fig. 3).
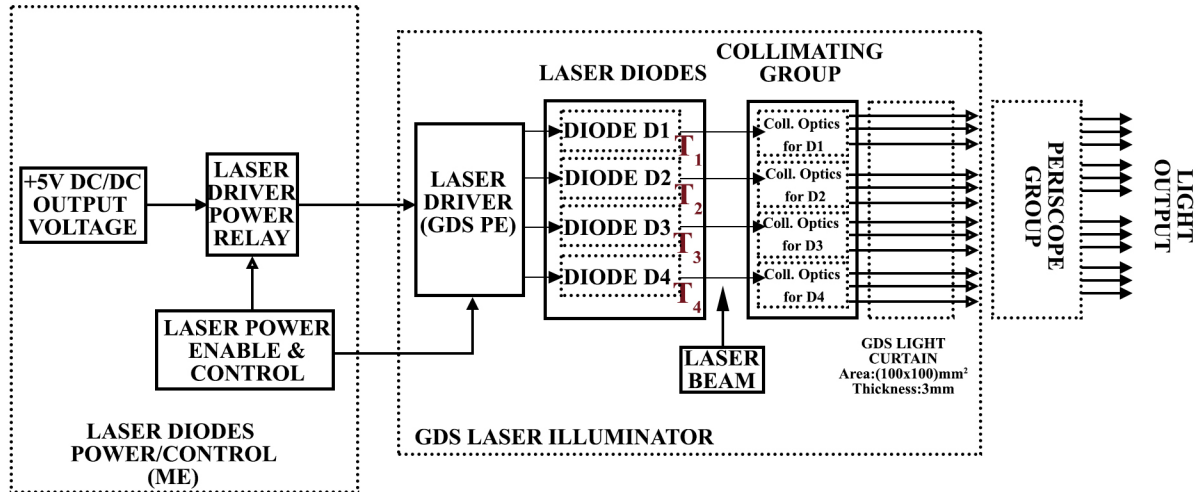
Fig. 2: The laser illuminator subsystem and its power supply block diagram (modified from Calamai et al., 2000).
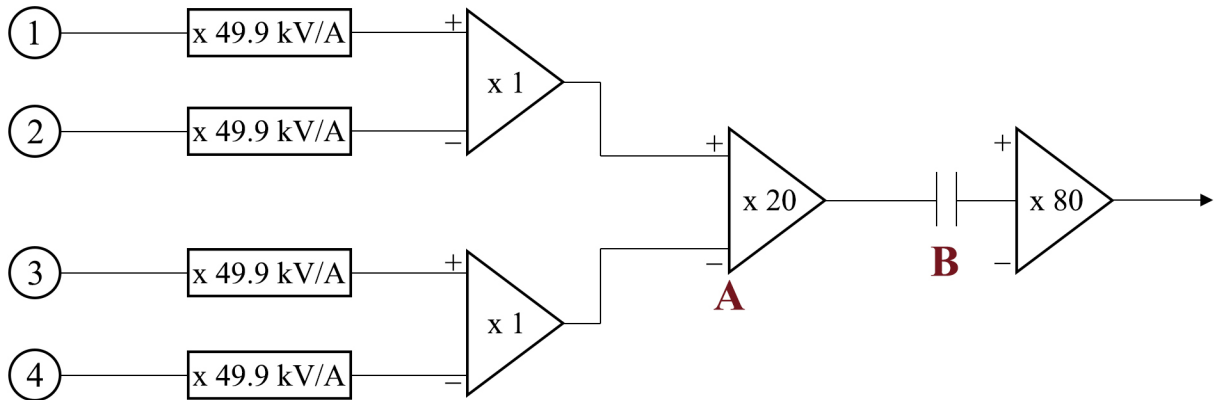

Fig. 3: Diagram of the proximity electronics of one of the two GDS receivers. The photodiode signals are converted into voltage and subtracted from the adjacent photodiodes, then the two resulting voltages are subtracted at the second amplification stage, where the signal is amplified 20 times (A). The capacitive coupling (B) between the second and the third stage eliminates the DC component of the signal and keeps the 100 kHz modulated component scattered by the dust particle crossing the laser curtain (modified from Epifani, 2000a).

The IS (Esposito et al., 2002) consists of five lead zirconate titanate ceramic piezoelectric transducers (model PZT5A produced by Morgan Matroc with Curie Temperature $T_C = 365°C$), resonating at 200 kHz and installed under the centre and below the four corners of a square aluminium plate (124 mm x 124 mm x 0.5 mm). The IS proximity electronics consist of five pre-processing circuits, one for each PZT. The signal, recorded by each PZT, is processed by a dedicated circuit (Esposito, 2001) and transferred to the main electronics where it is compared with the threshold set in a dedicated comparator (Vergara and Olivares, 2000). The IS is equipped with a sensor to monitor the plate temperature. An additional piezoelectric device (PZT_{Cal}) is placed under the plate between PZT1 and PZT5 (Fig. 4) to act as an internal calibrator monitoring the IS performance in time and at different environment conditions, e.g. operative temperatures. A voltage pulse of a pre-defined level, applied to PZT_{Cal}, produces the IS calibration stimulus. The calibration is applied periodically or triggered by ground telecommand. The voltage level and the number of stimuli are two settable parameters; the default values for periodic calibration are: calibration level = 10 V, and number of stimuli = 4. The PZT_{Cal} generates a mechanical stimulus to

the IS plate; the resulting bending wave propagates at 200 kHz along the plate and is detected by the five piezoelectric sensors. The PZTs sensitivity is monitored by analysing the measured signal amplitude and the time delays with respect to the first detecting PZT. The amplitudes and the time delays induced by the internal calibrator are recorded in the IS calibration telemetry packet.
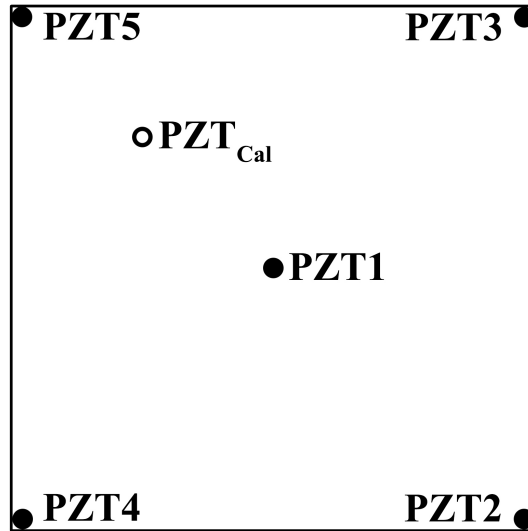

Fig. 4: Sketch showing the position of the five piezoelectric sensors plus the internal calibrator (PZT$_{Cal}$) under the plate of the IS.

The MBS subsystem consists of five microbalances MK21, produced by QCM Research, installed around the GIADA entrance and pointing in five different directions in order to characterize the dust flux within a view angle of 180° (Della Corte et al., 2016a). Each QCM is composed of two AT-cut quartz crystals (O'Sullivan and Guilbault, 1999), one exposed to the dust environment and the other, isolated from the dust environment, acting as reference, resonating at 15 MHz. The change of the beat frequency is related to the accumulated mass deposited on the exposed quartz crystal (Palomba et al., 2002). A heating device is installed on each QCM to monitor the frequency vs. temperature behaviour. These sensors are in general characterized by a temperature dependence (Battaglia et al., 2004; Palomba et al., 2002; Tighe et al., 2009); this issue can be solved by performing frequencies readings at fixed temperatures. **In order to evaluate the amount of mass accumulated on the QCMs, we identify for each of them the most recurrent temperature registered (reference temperatures) and we consider the frequency readings only when it occurs (Della Corte et al., 2015).** The heating device can be also used to sublimate any volatile component deposited on the quartz sensors.

3. Data Analysis

3.1 Grain Detection System receivers

For each GDS receiver (Left and Right channels), two quantities are measured independently every hour and recorded in the GDS calibration telemetry: the mean noise signal ("GDS mean") and its standard deviation ("GDS standard deviation"). **These are evaluated, for each receiver, over a sample of 32 measurements acquired in about 1 second, i.e. a time interval during which it is highly improbable that the detection of a dust particle occurs.** The GDS mean values recorded during the period under study are reported in Fig. 5.
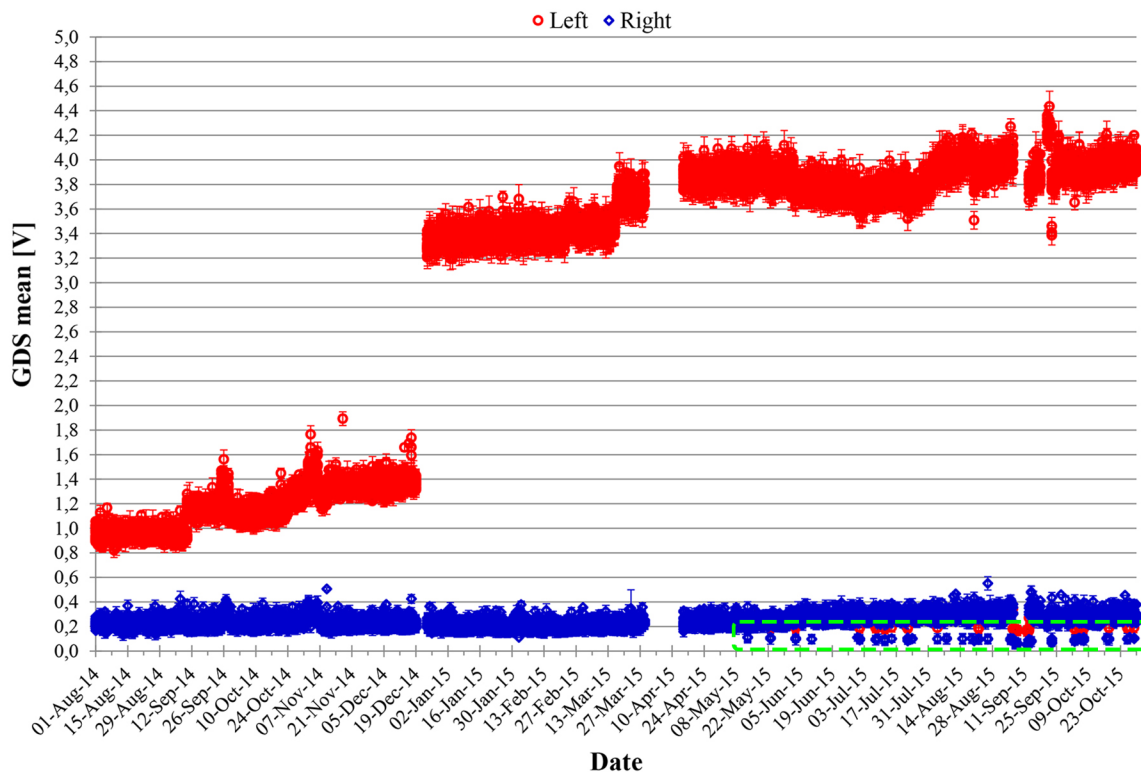
Fig. 5: Noise signal (GDS mean) for the Left (circles) and Right (diamonds) GDS receivers collected from 1 August 2014 to 31 October 2015. The Left receiver data < 0.2 V and the Right receiver data < 0.1 V, enclosed in the dashed rectangle (bottom right), correspond to the saturation of the GDS receivers (Della Corte et al., 2014).

On 1 August 2014, the mean noise level of the Left channel (circles in Fig. 5) was at ~1.0 V. This value is comparable to the one recorded at the end of the Rosetta cruise phase and confirms the Left channel increase of noise level occurred after payload checkout 9 (Della Corte et al., 2014). The noise level of this channel significantly increased during the mission. Probably this was due to dust contamination of the GDS optics, e.g. periscope group (Epifani, 2000a), which induced an increase of the internal stray light. The first significant noise step occurred on 20 December 2014, when the signal increased from about 1.4 V to ~3.3 V. The contamination could be due to a "dust shower" (Fulle et al., 2015), but this cannot be confirmed as the GDS subsystem was switched off for four hours on 20 December 2014. On 16 March 2015 the noise increased from ~3.4 V up to ~3.7 V, when a high dust detection rate was registered. On 29 March 2015, the Rosetta spacecraft went to "Safe Mode" switching off all the instruments, including GIADA. During the emergency switch off procedure the GIADA cover was closed. When GIADA was switched on again on 14 April 2015 the noise was at ~3.9 V. The contamination could be due to dust accumulated in the GIADA cover during the previous months of measurements and falling onto the GDS optics when the cover was closed. The hypothesis that the noise increase was due to the dust deposited onto the GDS optics is supported by the noise trend recorded between 17 July 2015 and 14 August 2015, i.e. around perihelion when the dust detection rate was high.

On 7 September 2015 the laser temperatures increased, with values near to their soft-limits, due to the illumination conditions. In order to avoid over stress to the GDS, the subsystem was switched off from 8 to 12 September. At the following GDS switch on a slightly lower noise level (~3.8 V) was observed. This was due to the higher laser temperature, which results in a lower light intensity (Section 3.2) and a consequent stray light decrease in the receivers. An issue with the Rosetta spacecraft Solid State Mass Memory (SSMM) occurred on 15 September 2015. To perform

the recovery actions GIADA was off with the cover open, from the 18 to 21 September. When GIADA was switched on the noise level was at ~4.2 V and after a series of fluctuations it stabilised at ~4.0 V, on 31 October 2015. This behaviour was due to the trend of the laser temperature induced by the specific observing geometry.

The mean noise level of the Right channel (diamonds in Fig. 5) is generally lower than for the Left channel and does not show significant increases. **The tests carried out on the GDS receivers during the on-ground calibration activity (Epifani, 2000a) and the analysis of the data acquired during the cruise phase (Della Corte et al., 2014) showed that the Right channel was less affected by stray light than the Left one. This was due to a lower light intensity of the laser mounted close to the Right channel with respect to the light intensity of the laser installed close to the Left channel**. For the whole period under study only a slight increase from ~0.2 V to ~0.3 V was registered on the Right channel, which produced negligible effects on its performance. On the contrary, the noise increase for the Left receiver affected the sensitivity range of the measurable particle cross sections, reducing its upper limit to 24% of the original value. Despite this, the GDS was still able to detect and measure every individual particle crossing the laser curtain for the entire period of the Rosetta scientific operations.

As explained by Della Corte et al. (2014), the GDS receivers can be saturated by direct Solar illumination at Rosetta - Sun distances lower than 2 au. This is the case for the data enclosed in the dashed rectangle reported in Fig. 5, where the mean noise levels of both the Left and Right receivers are lower than 0.2 V and 0.1 V, respectively. The low noise values are produced by the saturation of the second amplification stage (A in Fig. 3); this continuous signal is cut by the capacitive coupling (B in Fig. 3).

3.2 Laser light emission

We analysed the light emitted by each of the four laser photodiodes as a function of the laser operative temperature, during the period 1 August 2014 – 31 October 2015. The almost linear relation between the laser emitted light and the operative temperature is nominal and similar those observed during the Rosetta cruise phase (Della Corte et al., 2014) and during on-ground calibration (Epifani, 2000b). Fig. 6 shows as an example the laser 1 emitted light versus its operative temperature.
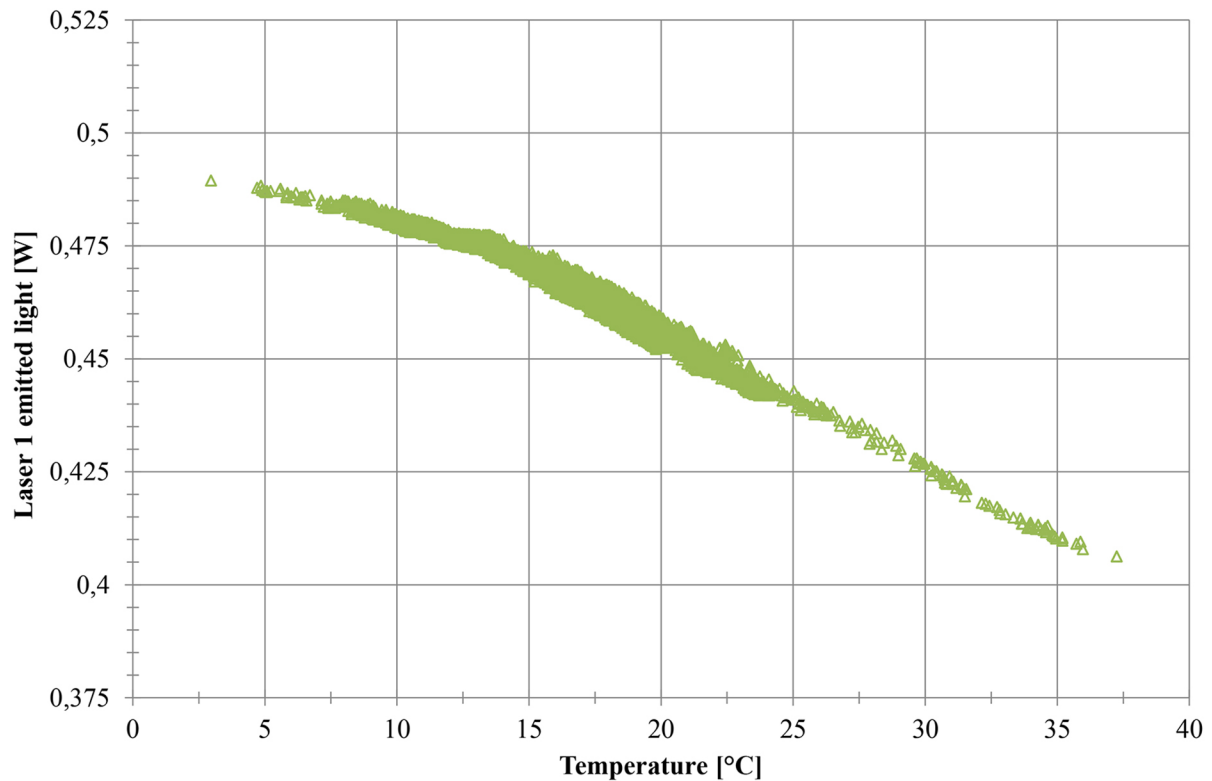
Fig. 6: Laser 1 emitted light versus the operative temperature. The linear trend indicates nominal laser behaviour.

We investigated the effect of the laser light emission variations on the measurement of the dust particle cross section. A reduction in the laser light emission implies that a particle crossing the laser curtain is illuminated with a lower light intensity and thus scatters a smaller amount of light, hence mimicking the behaviour of a particle with smaller cross section. Characterising the laser light emission as a function of the temperature is critical to constrain the measurement error on the particle cross section. To define and evaluate this error we ran a dedicated test on the GIADA Proto Flight Model (hereafter GIADA PFM, Fig. 1), available on-ground and operated in a clean room in our laboratory (Della Corte et al., 2016a). The laser emitted light measured by GIADA in flight until 20 December 2014, i.e. when the first significant GDS receiver contamination occurred, showed a maximum laser emitted light variation of ~44 mW, due to the operative temperatures. To reproduce a similar laser emitted light variation on GIADA PFM we **increased** the lasers' power **by** about 16%. We simulated the particle crossing using a thin glass needle placed in the laser curtain. Such a power variation induced a maximum GDS signal variation of about 5%. Since the cross section is proportional to the square of the scattered light signal (Della Corte et al., 2016a), the maximum uncertainty induced by laser emitted light variations on the particle cross section measurements is about 10%. These uncertainties are negligible within the procedure we followed to obtain the calibration curves (Della Corte et al., 2016a) necessary to derive the particle cross section.

3.3 Impact Sensor

The IS internal calibrator (PZT$_{Cal}$) can be used to check the behaviour of the IS subsystem, in particular of the signal amplitude and the bending wave propagation times over the sensing plate (time delays). To evaluate the IS performance from August 2014 until October 2015 we calculated the mean and the standard deviation for all the calibration measurements performed. As an example, we report the results obtained for five months of the whole studied period (Fig. 7). The calibrator signal amplitude mean values are reported in Fig. 7a; the standard deviations are not visible in the plot because they are negligible. These results show a very stable behaviour of the

piezoelectric transducers: the measured signal amplitudes do not vary, except for PZTs 3 and 5 that show some minor fluctuations, i.e. well below 2% of the signal average value recorded during the entire period under study. The time delays measured by the counters linked to the five piezoelectric transducers are plotted in Fig. 7b. The average time delay values remain constant except for PZT3 which shows a small variability. However, this variation is insignificant; in fact, it is smaller than the time resolution of the counter (3 µs).

The electrical noise of the IS acquisition chain during the studied period remains constant: the rate of spurious detections due to spikes or electrical noise does not show any variation.
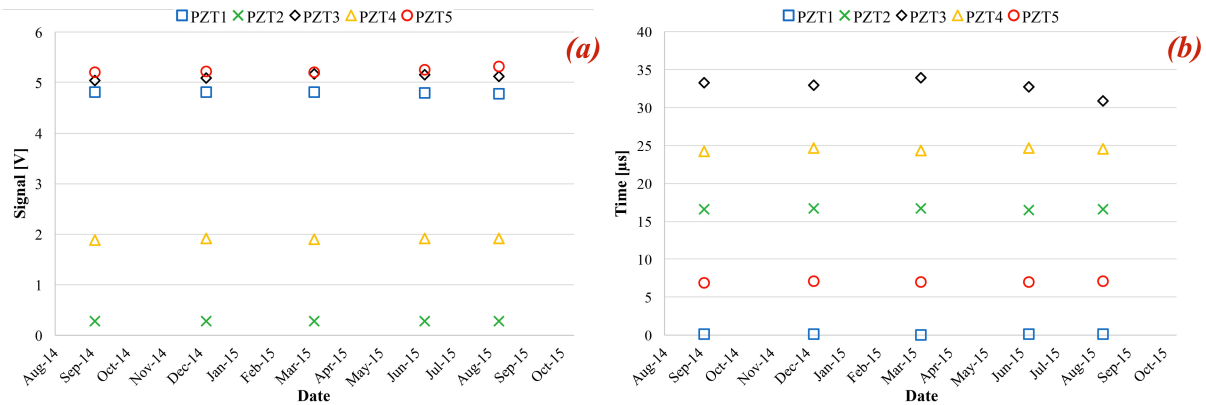

Fig. 7: IS internal calibrator signal amplitude means (a) and time delay mean values (b) for selected months, for each of the five piezoelectric transducers. **Each plotted value represents the average of signal amplitudes and time delays, calculated over the whole selected month.**

For the whole considered period, the signals recorded by the 5 PZTs sensors didn't show any significant systematic variations, leading us to conclude that the PZT_{Cal} did not suffer any performance degradation due to age or operative temperature variation. If a PZT_{Cal} decrease in performance had occurred, due to sensor ageing or operating temperatures, we would expect to observe the same behaviour also on the other PZTs, resulting in significant variations of their signals prompted by the calibration stimulus. Indeed, in case of a lower piezoelectric conversion efficiency, PZT_{Cal} would produce less intense stimuli on the IS plate, the other PZTs would respond less to the stresses and so the effect would result in weaker PZTs output signals.

3.4 IS Cross-talk

We performed calibration activities on the IS GIADA PFM in the laboratory (Della Corte et al. 2016a). Since we noted that the PZT2 sensor showed a non-nominal behaviour it was studied in depth, stimulating the IS plate with different PZT_{Cal} amplitudes and by applying different PZT2 threshold values (Fig. 8a). Setting the PZT2 threshold to values lower than 280 mV, the higher the PZT_{Cal} stimulus the lower the PZT2 signal (Fig. 8a). We find that the recorded time delays (

Tab. **1**, GIADA PFM) are lower than the theoretical value (51 µs), which is estimated considering the geometrical configuration of the PZT sensors (Fig. 4) and assuming a constant wave propagation speed of 1.711 mm µs^{-1} (Esposito et al., 2002). When the threshold is set to 280 mV the signal rises linearly up to a stimulus of 6 V and then decreases (Fig. 8a). With the highest threshold value and for stimuli of 7 V, we obtained a time delay close to the theoretical value (

Tab. **1**, GIADA PFM). **In this configuration, performing a best fit on the data up to 6 V, we can estimate the PZT2 expected signal (about 3.2 V) for the highest stimulus. The signal detected by PZT2, for highest amplitude stimulus, is instead ~1.5 V, lower than the expected one. With a threshold lower than 280 mV, the PZT2 detected signal drops to 0.4 V (**Fig. 8a**).** All these considerations led us to conclude that GIADA PFM PZT2 is affected by **electrical** cross-talk, i.e. a signal detected by another PZT creates an undesired effect on PZT2. The analysis of the

time delays measured during the cruise phase for the GIADA in flight PZT2 (Della Corte et al., 2014) provided first evidence that it was affected by **electrical** cross-talk. In order to verify this behaviour, we performed a dedicated test on GIADA in flight, reproducing the tests performed on GIADA PFM in the laboratory. We used three different PZT_{Cal} amplitudes and three different threshold values. The signals recorded by PZT2 on GIADA in flight are reported in Fig. 8b. The test confirmed the non-nominal behaviour for the PZT2 in flight. Only when the threshold is set to 280 mV the PZT2 signal (Fig. 8b) increases linearly with the stimulus, but the time delays recorded are always inaccurate. The time delays recorded with low threshold values are always shorter than the theoretical delays (

Tab. **1**, GIADA); the results demonstrated that the inflight PZT2 sensor is also affected by **electrical** cross-talk. The full characterisation of the PZT2 behaviour allowed us to improve the accuracy in the reconstruction of the impact position of a particle impinging on the IS plate by 25% (Della Corte et al., 2016a).
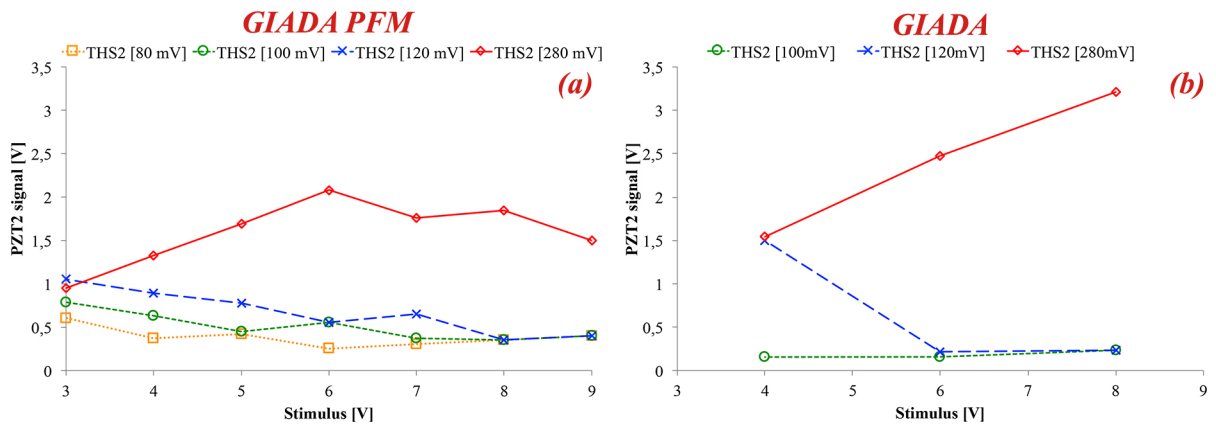

Fig. 8: (a) PZT2 signals on GIADA PFM in the laboratory vs. PZT_{Cal} stimulus at different thresholds (THS2); (b) PZT2 signals on GIADA in flight vs. PZT_{Cal} stimulus at different THS2.

Stimulus [V]	GIADA PFM (in the laboratory)								GIADA (in flight)					
	PZT2 Thresholds								PZT2 Thresholds					
	80 mV		100 mV		120 mV		280 mV		100 mV		120 mV		280 mV	
	t [µs]	Δt [µs]	t [µs]	Δt [µs]	t [µs]	Δt [µs]	t [µs]	Δt [µs]	t [µs]	Δt [µs]	t [µs]	Δt [µs]	t [µs]	Δt [µs]
3	42	-9	48	-3	63	12	69	18	-	-	-	-	-	-
4	30	-21	36	-15	42	-9	63	12	48	-3	72	21	87	36
5	30	-21	30	-21	36	-15	63	12	-	-	-	-	-	-
6	27	-24	33	-18	33	-18	63	12	33	-18	36	-15	78	27
7	27	-24	27	-24	30	-21	48	-3	-	-	-	-	-	-
8	27	-24	27	-24	27	-24	42	-9	33	-18	30	-21	72	21
9	27	-24	30	-21	30	-21	39	-12	-	-	-	-	-	-

Tab. 1: Time delays (t) recorded by the PZT2 sensors on GIADA PFM in the laboratory (left) and on GIADA in flight (right), at different thresholds and using different stimuli for the internal calibrator. Δt is the

difference between the recorded time delay and the theoretical time delay (51 µs), estimated considering the geometrical configuration of the PZT sensors and assuming a constant wave propagation speed of 1.711 mm µs^{-1} (Esposito et al., 2002).

3.5 Micro-balances system

In order to monitor the five QCMs responses we analysed the frequency behaviour vs. temperature during the heating process. As an example in Fig. 9, we report the frequency vs. temperature trend for *QCM5,* recorded during four different heating processes performed during the cruise phase, March 2004 – June 2011 **(Fig. 9a)**, and during the Rosetta scientific phase, May 2014 – September 2016 **(Fig. 9b)**. The curve trends are similar, showing only an upper shift in frequency due to dust collection. The same behaviour has been observed for all the QCMs. The stability of frequency vs. temperature curves indicates a nominal behaviour of the five microbalances along the entire mission.
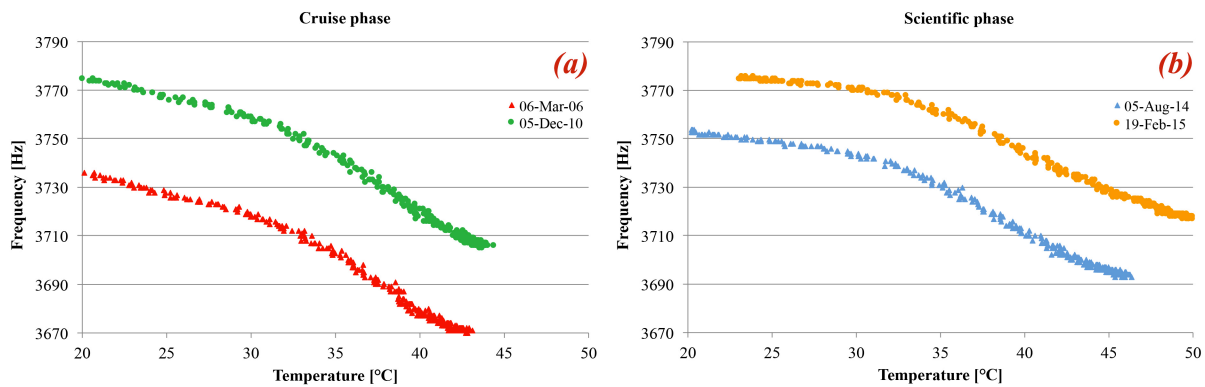

Fig. 9: **QCM5 frequency vs. temperature during the active heating process performed during the Rosetta cruise (a) and scientific (b) phases. The trend of these curves is in accordance with typical behaviour for AT-cut QCM (Sauerbrey, 1959) and comparable with the frequency vs temperature curves provided by the QCM manufacturer.**

4. Conclusions

The GIADA inflight calibration data recorded from 1 August 2014 to 31 October 2015 were analysed in order to evaluate GIADA performance throughout this period of the Rosetta mission. We observed that the noise in one of the two GDS receivers (Left receiver) increased during the considered period. This effect is attributed to dust contamination on the GDS optics. The noise increase did not prevent GDS nominal operations. The only consequence was a reduced sensitivity, with consequent reduction of the maximum dust particle cross section measurable by the Left receiver. The lasers' light emission maintained the nominal behaviour despite some variations due to operative temperature changes, which did not introduce additional uncertainties in the measurement of the dust particle cross sections.

The tests performed on GIADA in flight and on GIADA PFM confirmed that the PZT2 sensors of both GIADA models are affected by cross-talk. Taking into account this issue, the work performed during the extended calibration activity (Della Corte et al., 2016a) allowed to improve the accuracy of the dust particle impact position reconstruction. The analysis of the signal and of the time delays recorded by the five PZTs, as a result of the IS calibrations, shows that the IS maintained a nominal behaviour during the whole examined period, with a good stability with respect to the different observation conditions.

The MBS data obtained during the heating process demonstrate that the QCM frequency vs.

temperature trends did not change.

We conclude that during the 86 months of cruise and the investigated 15 months of operation GIADA operated under nominal conditions.

Acknowledgements

References

Auer, S. and Sitte, K. 1968. Detection technique for micrometeoroids, using impact ionization. Earth Planet. Sci. Lett. 4, 178-183, doi: 10.1016/0012-821X(68)90013-7.

Battaglia, R., Palomba, E., Palumbo, P., Colangeli, L., Della Corte, V. 2004. Development of a micro-balance system for dust and water vapour detection in the Mars atmosphere. Adv. Space Res. 33, 2258-2262, doi: 10.1016/S0273-1177(03)00520-9.

Berlincourt, D., Krueger, H. A., Near, C. 2000. Properties of Morgan electro ceramic ceramics. Technical Publication TP-226, Morgan Electro Ceramics.

Berger, O. E. and Richardson, F. F. 1969. The Pioneer 8 Cosmic Dust Experiment. Rev. Sci. Instrum. 40, 1333-1337, doi: 10.1063/1.1683778.

Calamai, L., Cherubini., G., Cosi, M., Giunti, C., Farulli, L. 2000. GIA-GAL-TN-507. Technical note Officine Galileo, Firenze.

Colangeli L., Lopez Moreno J. J., Palumbo P., Rodriguez J., Bussoletti E., Della Corte V., Esposito F., Herranz M., Jeronimo J. M., Lopez-Jimenez A., Epifani E. M., Morales R., Palomba E., Rotundi A., Vergara S., International GIADA Team 2007., GIADA: The Grain Impact Analyser and Dust Accumulator for the Rosetta space mission. Adv. Space Res. 39, 446–450, doi: 10.1016/j.asr.2006.12.048.

Della Corte, V., Rotundi, A., Accolla, M., Sordini, R., Palumbo, P., Colangeli, L., Lopez Moreno, J. J., Rodriguez, J., Rietmeijer, F. J. M., Ferrari, M., Lucarelli, F., Mazzotta Epifani, E., Ivanovski, S., Aronica, A., Cosi, M., Bussoletti, E., Crifo, J. F., Esposito, F., Fulle, M., Green, S. F., Gruen, E., Herranz, M. L., Jeronimo, J. M., Lamy, P., Lopez Jimenez, A., McDonnell, J. A. M., Mennella, V., Molina, A., Morales, R., Moreno, F., Palomba, E., Perrin, J. M., Rodrigo, R., Weissman, P., Zakharov, V., Zarnecki, J. C. 2014. Giada: its Status after the Rosetta Cruise Phase and On-Ground Activity in Support of the Encounter with Comet 67P/Churyumov-Gerasimenko. J. Astron. Instrum. 3, 1350011, doi: 10.1142/S2251171713500116.

Della Corte, V., Rotundi, A., Fulle, M., Gruen, E., Weissmann, P., Sordini, R., Ferrari, M., Ivanovski, S., Lucarelli, F., Accolla, M., Zakharov, V., Mazzotta Epifani, E., Lopez-Moreno, J. J., Rodriguez, J., Colangeli, L., Palumbo, P., Bussoletti, E., Crifo, J. F., Esposito, F., Green, S. F., Lamy P. L.,

McDonnell, J. A. M., Mennella, V., Molina, A., Morales, R., Moreno, F., Ortiz J. L., Palomba, E., Perrin, J. M., Rietmeijer, F. J. M., Rodrigo, R., Zarnecki, J. C., Cosi, M., Giovane, F., Gustafson, B., Herranz, M. L., Jeronimo, J. M., Leese, M. R., Lopez-Jimenez, A. C. and Altobelli, N. 2015. GIADA: shining a light on the monitoring of the comet dust production from the nucleus of 67P/Churyumov-Gerasimenko. Astron. Astrophys. 583, A13, doi: 10.1051/0004-6361/201526208.

Della Corte, V., Sordini, R., Accolla, M., Ferrari, M., Ivanovski, S., Rotundi, A., Rietmeijer, F.J.M., Fulle, M., Mazzotta-Epifani, E., Palumbo, P., Colangeli, L., Lopez-Moreno, J. J., Rodriguez, J., Morales, R., Cosi, M. 2016a. GIADA - Grain Impact Analyzer and Dust Accumulator - onboard Rosetta spacecraft: extended calibrations. Acta Astronautica 126, 205-214, doi: 10.1016/j.actaastro.2016.03.036.

Della Corte, V., Rotundi, A., Fulle, M., Ivanovski, S., Green, S. F., Rietmeijer, F. J. M., et al., 2016b. 67P/CG Inner Coma dust properties from 2.2 au inbound to 2.0 au outbound to the Sun. Mon. Not. Roy. Astr. Soc. 462, S210-S219, doi: 10.1093/mnras/stw2529.

Dietzel, H., Eichhorn, G., Fechtig, H., Grün, E., Hoffmann, H.-J., Kissel, J. 1973. The HEOS 2 and HELIOS micrometeoroid experiments. J. Phys. E: Sci. Instrum. 6, 209–217, doi: 10.1088/0022- 3735/6/3/008.

Epifani, E. 2000a. La missione Rosetta verso la cometa 46P/Wirtanen: sviluppo, realizzazione e test del sistema di rivelazione grani GDS per lo strumento GIADA **(Rosetta mission to comet 46P / Wirtanen: development, implementation and testing of GDS grain detection system for the GIADA instrument)**. PhD Thesis, Università degli Studi di Napoli "Federico II".

Epifani, E. 2000b. RO-GIA-IUNOAC-TR-021. Technical report Osservatorio Astronomico di Capodimonte.

Esposito, F. 2001. Il sensore d'Impatto dello strumento GIADA per la misura della quantità di moto di grani cometary della sonda spaziale ESA "ROSETTA" **(The Impact Sensor of the GIADA instrument for measuring the momentum of cometary grains of the ESA "ROSETTA" space probe)**. PhD Thesis, Università degli Studi di Napoli "Federico II".

Esposito, F., Colangeli, L., Della Corte, V., Palumbo, P. 2002. Physical aspect of an "impact sensor" for the detection of cometary dust momentum onboard the "Rosetta" space mission. Adv. Space Res. 29, 1159–1163, doi: 10.1016/S0273-1177(02)00132-1.

Fulle, M., Della Corte, V., Rotundi, A., Weissman, P., Juhasz, A., Szego, K., Sordini, R., Ferrari, M., Ivanovski, S., Lucarelli, F., et al. 2015. Density and charge of pristine fluffy particles from comet 67p/Churyumov– Gerasimenko. Astrophys. J. Lett. 802, L12, doi: 10.1088/2041-8205/802/1/L12.

Fulle, M., Marzari, F., Della Corte, V., Fornasier, S., Sierks, H., Rotundi, A., et al., 2016a. Evolution of the Dust Size Distribution of Comet 67P/Churyumov–Gerasimenko from 2.2 au to Perihelion. Astrophys. J. 821, 19, doi: 10.3847/0004-637X/821/1/19.

Fulle, M., Della Corte, V., Rotundi, A., Rietmeijer, F. J. M., Green, S. F., Weissman, P., et al., 2016b. Comet 67P/Churyumov-Gerasimenko preserved the pebbles that formed planetesimals. Mon. Not. Roy. Astr. Soc. 462, S132-S137, doi: 10.1093/mnras/stw2299.

Grün, E., Fechtig, H., Giese, R.H., Kissel, J., Linkert, D., Maas, D., McDonnell, J. A. M., Morfill, G.E., Schwehm, G. and Zook, H. A. 1992a. The Ulysses dust experiment. Astron. Astrophys. Suppl. Ser. 92, 411-423.

Grün, E., Fechtig, H., Hanner, M.S., Kissel, J., Lindablad, B.-A., Linkert, D., Maas, D., Morfill, G. E. and Zook, H. A. 1992b. The Galileo dust detector. Space Sci. Rev. 60, 371-340.

Grün, E., Agarwal, J., Altobelli, N., Altwegg, K., Bentley, M. S., Biver, N., et al., 2016. The 19 Feb. 2016 Outburst of Comet 67P/CG: An ESA Rosetta Multi-Instrument Study. Mon. Not. Roy. Astr. Soc. 462, S220-S234, doi: 10.1093/mnras/stw2088.

Horányi, M., Hoxie, V., James, D., Poppe, A., Bryant, C., Grogan, B. Lamprecht, B., Mack, J., Bagenal, F., Batiste, S., Bunch, N., Chanthawanich, T., Christensen, F., Colgan, M., Dunn, T., Drake, G., Fernandez, A., Finley, T., Holland, G., Jenkins, A., Krauss, C., Krauss, E., Krauss, O., Lankton, M., Mitchell, C., Neeland, M., Reese, T., Rash, K., Tate, G., Vaudrin, C. and Westfall, J. 2008., The Student Dust Counter on the New Horizons mission. Space Sci. Rev. 140, 387-402, doi: 10.1007/s11214-007-9250-y.

Humes, D. H. 1980. Results of Pioneer 10 and 11 meteoroid experiments: Interplanetary and near‐Saturn. J. Geophys. Res.: Space Physics 85, 5841-5852, doi: 10.1029/JA085iA11p05841.

Landis, G. A., Jenkins, P., Flatico, J., Oberle, L., Krasowski, M. and Stevenson, S. 1996. Development of a Mars dust characterization instrument. Planet. Space Sci. 44, 1425-1433, doi: 10.1016/S0032-0633(96)00042-6.

Leese, M. R., McDonnell, J. A. M., Burchell, M. J., Green, S. F., Jolly, H. S., Ratcliff, P. R. and Shaw H. A.

1996. DEBIE: a Low Resource Dust Environment Monitor. In ESA Symposium Proceedings on "Space Station Utilisation". ESA SP-385, 417-420.

Mazzotta Epifani, E., Bussoletti, E., Colangeli, L., Palumbo, P., Rotundi, A., Vergara, S., Perrin J.M., Lopez Moreno J.J. and Olivares, I. 2002. The grain detection system for the GIADA instrument: design and expected performances. Adv. Space Res. 29, 1165-1169, doi: 10.1016/S0273-1177(02)00133-3.

McDonnell, J.A.M., 1969. Calibration studies on a piezoelectric sensing diaphragm for the detection of micrometeorites in space. J. Phys. E: Sci. Instrum. 2, 1026-1030, doi: 10.1088/0022-3735/2/12/304.

McDonnell, J.A.M., 1978. Microparticle Studies by Space Instrumentation. In Cosmic dust (Ed. J.A.M. McDonnell), John Wiley and Sons, New York, 337-426.

McDonnell, J.A.M. 1987. The Giotto dust impact detection system. J. Phys. E: Sci. Instrum. 20, 741-758, doi: 10.1088/0022-3735/20/6/033.

McKeown, D. 1998. Quartz crystal instrumentation for space research, Proc. SPIE 3427, Optical Systems Contamination and Degradation, **113-125,** doi: 10.1117/12.328483.

Nakamura, Y., Nishijo, K., Murakami, N., Kawashima, K., Horikawa, Y., Yamamoto, K., Ohtani, T., Takashi, Y. and Inoue K. 2013. Small Demonstration Satellite-4 (SDS-4): Development, Flight Results, and Lessons Learned in JAXA's Microsatellite Project. In 27th Annual AIAA/USU Conference on Small Satellites**, SSC13-X-1**, **1-15**.

O'Neal, R. L. 1974. Description of the meteoroid detection experiment flown on the Pioneer 10 and 11 Jupiter flyby missions. NASA technical note, NASA-TN-D-7691, L-9517.

O'Sullivan, C. K. and Guilbault, G. G. 1999. Commercial quartz crystal microbalances–theory and applications. Biosensors and bioelectronics 14.8, 663-670, doi: 10.1016/S0956-5663(99)00040-8.

Palomba, E., Colangeli, L., Palumbo, P., Rotundi, A., Perrin, J. M., Bussoletti, E. 2002. Performance of micro-balances for dust flux measurement. Adv. Space Res. 29, 1155–1158, doi: 10.1016/S0273-1177(02)00131-X.

Pankove, J. I. 1968. Temperature dependence of emission efficiency and lasing threshold in laser diodes. IEEE Journal of Quantum Electronics 4, 119-122, doi: 10.1109/JQE.1968.1075062.

Rotundi, A., Sierks, H., Della Corte, V., Fulle, M., Gutierrez, P. J., Lara, L., Barbieri, C., Lamy, P. L., Rodrigo, R., Koschny, D., et al. 2015. Dust measurements in the coma of comet 67P/Churyumov-Gerasimenko inbound to the Sun. Science 347 6220, doi: 10.1126/science.aaa3905.

Sabat, R. G., Mukherjee, B. K., Ren, W. and Yang, G. 2007. Temperature dependence of the complete material coefficients matrix of soft and hard doped piezoelectric lead zirconate titanate ceramics. J. Appl. Phys.101, 064111, doi: 10.1063/1.2560441.

Sauerbrey, G. 1959. Verwendung von Schwingquarzen zur Wägung dünner Schichten und zur Mikrowägung. Z. Phys. 155, 206–222, doi: 10.1007/BF01337937.

Sherrit, S., Yang, G., Wiederick, H. D. and Mukherjee, B. K. 1999. Temperature dependence of the dielectric, elastic and piezoelectric material constants of lead zirconate titanate ceramics. In Proceedings of the International conference on smart materials, structures and systems, 7-10.

Simpson, J. A. and Tuzzolino, A. J. 1985. Polarized polymer films as electronic pulse detectors of cosmic dust particles. Nucl. Instrum. Meth. A 236, 187-202, doi: 10.1016/0168-9002(85)90145-7.

Simpson, J. A., Rabinowitz, D., Tuzzolino, A. J., Ksanfomality, L. V. and Sagdeev, R. Z. 1987. The dust coma of comet P/Halley: measurements on the Vega-1 and Vega-2 spacecraft. Astron. Astrophys. 187, 742-752.

Soares, C.E., Barsamian, H., Rauer, S. 2002. Thruster-plume-induced contamination measurements from the PIC and SPIFEX flight experiments. Proc. SPIE 4774, Optical System Contamination: Effects, Measurements, and Control VII, **199-209**, doi: 10.1117/12.481653.

Srama, R., Ahrens, T. J., Altobelli, N., Auer, S., Bradley, J. G., Burton, M., Dikarev, V. V., Economou, T., Fechtig, H., Görlich, M., Grande, M., Graps, A., Grün, E., Havnes, O., Helfert, S., Horányi, M., Igenbergs, E., Jessberger, E. K., Johnson, T. V., Kempf, S., Krivov, A. V., Krüger, H., Mocker-Ahlreep, A., Moragas-Klostermeyer, G., Lamy, P., Landgraf, M., Linkert, D., Linkert, G., Lura, F., McDonnell, J. A. M., Möhlmann, D., Morfill, G. E., Müller, M., Roy, M., Schäfer, G., Schlotzhauer, G., Schwehm, G. H., Spahn, F., Stübig, M., Svestka, J., Tschernjawski, V., Tuzzolino, A. J., Wäsch, R., Zook, H. A. 2004. The Cassini Cosmic Dust Analyzer. Space Sci. Rev. 114, 465–518, doi: 10.1007/s11214-004-1435-z.

Tighe, A.P., Iwanosky, B., Van Eesbeek, M., Duzellier, S., Dinguirard, M., Falguere, D., Pons, C., Inguimbert, V., Rejsek, V., Durin, C. and Mandeville J.C. 2009. Overview of results from the

materials exposure and degradation experiment (MEDET) after 18 months in orbit on the ISS. Proceedings of the 11th ISMSE, Aix en Provence.

Tuzzolino, A. J., McKibben, R. B., Simpson, J. A., BenZvi, S., Voss, H. D. and Gursky, H. 2001. The Space Dust (SPADUS) instrument aboard the Earth-orbiting ARGOS spacecraft: I-instrument description. Planet. Space Sci. 49, 689-703, doi: 10.1016/S0032-0633(01)00012-5.

Tuzzolino, A. J., Economou, T. E., McKibben, R. B., Simpson, J. A., McDonnell, J. A. M., Burchell M. J., Vaughan, B. A. M., Tsou, P., Hanner, M. S., Clark, B. C., Brownlee, D. E. 2003. Dust Flux Monitor Instrument for the Stardust mission to comet Wild 2. J. Geophys. Res. (Planets) 108, E10, 8115, doi: 10.1029/2003JE002086.

Vergara, S. and Olivares, I. 2000. RO-GIA-RS-013 Requirement Specifications.

Wood, B. E., Green, B. D., Hall, D. F., Uy, O. M., Cain, R. P., Galica G. A., Boies, M. T. and Bertrand W. T. 2000. Update of the midcourse space experiment (MSX) satellite measurements of contaminant films using QCMs. Proc. SPIE 4096, Optical Systems Contamination and Degradation II: Effects, Measurements, and Control, doi:10.1117/12.400820.

Xiang, S.-B., Xiang, X., and Feng, C. G. 2009. Effects of temperature on laser diode ignition. Optik 120, 85-88, doi: 10.1016/j.ijleo.2007.06.013.

List of figure captions

Fig. 1: *(a)* GIADA, installed on the nadir panel of the Rosetta spacecraft, during the thermal test performed in 2002 in the Large Space Simulator at ESA's ESTEC facility, The Netherlands (Photo: ESA/A. Van Der Geest). *(b)* GIADA Proto Flight Model (GIADA PFM), operating in a clean room in our laboratory.

Fig. 2: The laser illuminator subsystem and its power supply block diagram (modified from Calamai et al., 2000).

Fig. 3: Diagram of the proximity electronics of one of the two GDS receivers. The photodiode signals are converted into voltage and subtracted from the adjacent photodiodes, then the two resulting voltages are subtracted at the second amplification stage, where the signal is amplified 20 times (A). The capacitive coupling (B) between the second and the third stage eliminates the DC component of the signal and keeps the 100 kHz modulated component scattered by the dust particle crossing the laser curtain (modified from Epifani, 2000a).

Fig. 4: Sketch showing the position of the five piezoelectric sensors plus the internal calibrator (PZT$_{Cal}$) under the plate of the IS.

Fig. 5: Noise signal (GDS mean) for the Left (circles) and Right (diamonds) GDS receivers collected from 1 August 2014 to 31 October 2015. The Left receiver data < 0.2 V and the Right receiver data < 0.1 V, enclosed in the dashed rectangle (bottom right), correspond to the saturation of the GDS receivers (Della Corte et al., 2014).

Fig. 6: Laser 1 emitted light versus the operative temperature. The linear trend indicates nominal laser behaviour.

Fig. 7: IS internal calibrator signal amplitude means (a) and time delay mean values (b) for selected months, for each of the five piezoelectric transducers. Each plotted value represents the average of signal amplitudes and time delays, calculated over the whole selected month.

Fig. 8: (a) PZT2 signals on GIADA PFM in the laboratory vs. PZT$_{Cal}$ stimulus at different thresholds (THS2); (b) PZT2 signals on GIADA in flight vs. PZT$_{Cal}$ stimulus at different THS2.

Fig. 9: QCM5 frequency vs. temperature during the active heating process performed during the Rosetta cruise (a) and scientific (b) phases. The trend of these curves is in accordance with typical behaviour for AT-cut QCM (Sauerbrey, 1959) and comparable with the frequency vs temperature curves provided by the QCM manufacturer.

List of table caption

Tab.1: Time delays (t) recorded by the PZT2 sensors on GIADA PFM in the laboratory (left) and on GIADA in flight (right), at different thresholds and using different stimuli for the internal calibrator. Δt is the difference between the recorded time delay and the theoretical time delay (51 μs), estimated considering the geometrical configuration of the PZT sensors and assuming a constant wave propagation speed of 1.711 mm μs-1 (Esposito et al., 2002).